ADVANCED MATERIALS
www.advmat.de

Traceable Nanoparticle Delivery of Small Interfering RNA and Retinoic Acid with Temporally Release Ability to Control Neural Stem Cell Differentiation for Alzheimer's Disease Therapy

Ran Zhang, Yan Li, Bingbing Hu, Zhiguo Lu, Jinchao Zhang, and Xin Zhang**

Alzheimer's disease (AD) is the most prevalent age-related neurodegenerative disorder.[1] The predominant pathologies of AD are gliosis and widespread neuronal loss, which progressively cause impairments in the memory and cognitive functions.[2] Current therapies, such as treatment with acetylcholinesterase inhibitors to enhance the cholinergic function, are inefficient due to the great hindrance at the blood–brain barrier (BBB) and their poor target ability to the diseased sites.[3] Therefore, it is necessary to develop more efficient methods to overcome these drawbacks.

Neural stem cells (NSCs) are becoming an increasingly attractive option because of their non-immunogenicity and ability to differentiate into neurons.[4] Generally, NSCs are stereotactically transplanted into the hippocampus of patients, which could avoid the interference of the BBB. Furthermore, NSCs have the capacity of targeting migration to the diseased sites after transplantation.[5] Therefore, these neurons could remedy the neuronal loss at the diseased site. However, there are two disadvantages limiting their application. Firstly, the differentiation of NSCs to neurons is far from successful because of their multi-directional differentiation.[6] It has been reported that only a small proportion of NSCs adopted a neuronal state after transplantation, while the majority differentiated into astrocytes.[7] Secondly, it is hard to track NSCs in real time after transplantation into the brain of patients, which is problematic as the therapeutic efficiency of NSCs depends on their transplantation site and their migration.[8] Therefore, the successful application of NSCs would be based on controlled differentiation of NSCs to neurons and long-term monitoring in real time.

For the aspect of controlling differentiation, retinoic acid (RA) has been proven to be capable of upregulating the expression of neuronal genes and inducing neuronal differentiation of NSCs.[9] Unfortunately, RA has a low solubility in aqueous solutions, which seriously impedes its application.[10] Furthermore, the neuronal promoting effect of RA was found to actually be counteracted by the SOX9 protein in NSCs, which suppresses neuronal gene expression and induces glial traits.[11] Therefore, it is necessary to down-regulate the expression of the SOX9 protein in advance to avoid its negative effect on RA. Small interfering RNA (siRNA) has been demonstrated as a great potential agent for the down-regulation of the gene expression via RNA interference (RNAi).[12] However, the intrinsic deficiencies of siRNA, such as the short plasma half-life and poor membrane penetrability, reduce its therapeutic efficiency.[13]

From the point of trackability, superparamagnetic iron oxide nanoparticles (SPIONs) have emerged for tracking the transplantation site and migration of NSCs thanks to their high relaxivity in magnetic resonance imaging (MRI).[14] Unfortunately, their effect is seriously limited due to the low permeability for the target cells.[15]

To this end, we intended to develop traceable nanoparticles (NPs) to satisfy the following conditions: 1) NPs that can load RA to enhance its solubility; 2) the system can form a complex with siSOX9 and achieve temporally controlled release, so that siSOX9 can be released earlier than RA to down-regulate the SOX9 protein expression; 3) SPIONs should be encapsulated and efficiently taken up by NSCs. To date, no such traceable NPs for AD have been reported. Prior studies have focused on either drug delivery or NSC monitoring. For instance, Santos and co-workers designed RA-loaded polymeric NPs as a tool to induce the neuronal differentiation of NSCs.[16a] Adams' group has used polymeric SPIONs for the MRI-based tracking of NSCs.[16b] Thus, it was important for us to make a proper balance between tracing NSCs in real time and offering enough neurons for alleviating AD.

NPs with complicated components have the potential to meet those conditions.[17] Amphiphilic cationic polymers or lipids could encapsulate hydrophobic SPIONs/drugs and complex siRNA. Neutral materials, such as polyethylene glycol (PEG), have been used to maintain the stability of such complexes. However, the steric hindrance due to PEGylation reduces the electrostatic interaction required for cellular uptake and

R. Zhang, Y. Li, B. Hu, Z. Lu, Prof. X. Zhang
National Key Laboratory of Biochemical Engineering
Institute of Process Engineering
Chinese Academy of Sciences
Beijing 100190, P. R. China
E-mail: xzhang@ipe.ac.cn
R. Zhang, Prof. J. Zhang
College of Chemistry & Environmental Science
Chemical Biology Key Laboratory of Hebei Province
Key Laboratory of Medicinal Chemistry and Molecular Diagnosis of the Ministry of Education
Hebei University
Baoding 071002, P. R. China
E-mail: jczhang6970@163.com
Z. Lu
University of Chinese Academy of Science
Beijing 100190, P. R. China

DOI: 10.1002/adma.201600554

ADVANCED MATERIALS
www.advmat.de

Materials Views
www.MaterialsViews.com

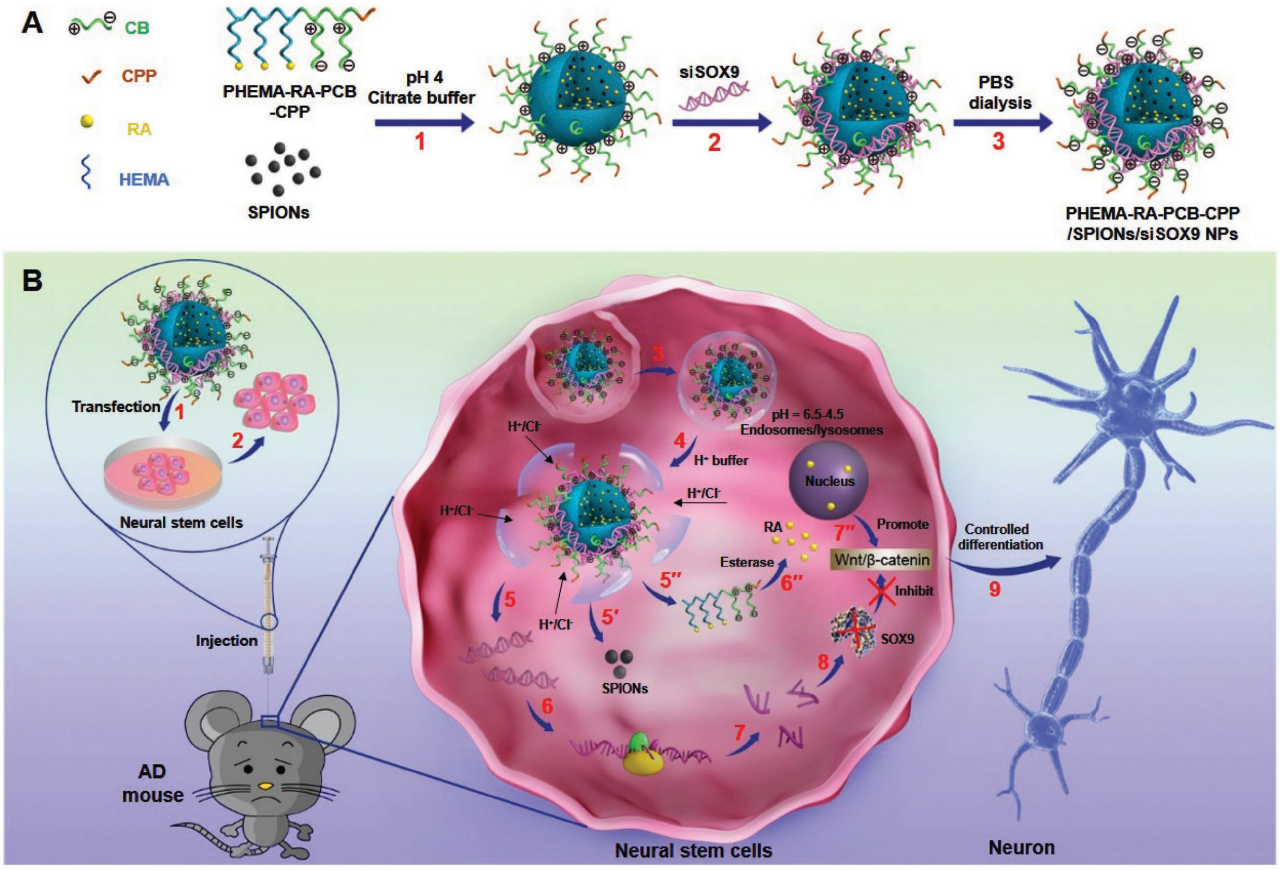

Scheme 1. A) Structural composition and preparation of the traceable NPs. PHEMA-RA-PCB-CPP polymers were self-assembled into NPs encapsulating SPIONs in the hydrophobic region (**1**). The NPs could complex siRNA in pH 4 citrate buffer because of the protonation of PCB (**2**) and revert to a neutral state after dialyzing in pH 7.4 PBS (**3**). B) Schematic diagram of cellular uptake and subcellular drug release of PHEMA-RA-PCB-CPP/SPIONs/siSOX9 NPs. NPs were added to the culture medium (**1**) and endocytosed by NSCs (**2**). In endosomes/lysosomes (**3**, **4**), siSOX9 (**5**), SPIONs (**5′**) and polymers (**5″**) were released into the cytoplasm. siSOX9 could inhibit the expression of SOX9 protein in advance (**6**, **7**, **8**), whereby RA was released sustainedly in the cytoplasm (**6″**). Free RA entering the nucleus upregulated the neuronal protein (**7″**), which could then control the differentiation of NSCs to neurons (**9**).

endosomal/lysosomal escape. Moreover, the multi-components generally impose an extra burden on the patient.[18] Therefore, the development of simple component NPs is urgently needed to be able to load SPIONs with a temporally controlled release ability of RA and siSOX9. In our previous study, we reported that the charge-reversible zwitterionic poly(carboxybetaine) (PCB) was neutral in physiological conditions and as such resisted nonspecific protein adsorption, which changed to a positive charge via protonation in acidic environment.[19] Inspired by this, we designed and synthesized PCB-based poly(2-hydroxyethyl methacrylate)-RA-poly(carboxybetaine) cell-penetrating peptide (PHEMA-RA-PCB-CPP) polymers to construct traceable, simple-component NPs for AD therapy.

As shown in **Scheme 1**A, PHEMA-RA-PCB-CPP polymers could self-assemble into NPs to encapsulate SPIONs in the hydrophobic region (**1**). The hydrophilic PCB could absorb siSOX9 in acidic environment to form a synergistic system (**2**) and the NPs reverted to the neutral state after dialysis (**3**). The CPP was conjugated to the outer layer of the NPs to enhance the interaction between the NPs and the NSCs for the promotion of endocytosis. As illustrated in Scheme 1B, after being endocytosed by the NSCs for transplantation, the NPs were expected to achieve the temporal release of siSOX9 and RA, such that siSOX9 was released first into the acting site to down-regulate the SOX9 protein expression in advance. RA was then sustainedly released into the cytoplasm and it thus efficiently controlled the differentiation of NSCs to neurons without the interference of the SOX9 protein. SPIONs were used to trace the transplantation site and migration of the NSCs though MRI. Therefore, the visualization of PHEMA-RA-PCB-CPP/SPIONs/siSOX9 NPs combined with NSCs would form an effective therapeutic and traceable system to alleviate AD.

The synthesis of the PHEMA-RA-PCB-CPP polymers is shown in Figure S1 (Supporting Information). The chemical structure of the obtained monomer and polymers was characterized by ^{1}H NMR (Figure S2, Supporting Information), which indicated their successful synthesis. For comparison, a PEG-2000-based PHEMA-RA-PEG-CPP polymer was also successfully synthesized (Figure S3, Supporting Information). The conjugation efficiency of CPP was studied by elemental analysis, which confirmed that all polymers were more than 10% conjugated (Table S3, Supporting Information). In

Adv. Mater. **2016**,
DOI: 10.1002/adma.201600554

the following studies, NPs with 10% CPP were prepared to investigate the effect on cellular uptake. The self-assembling ability of the polymers was evaluated by studying the critical micelle concentrations (CMCs). As shown in Figure S4 (Supporting Information), the CMC for the RA-conjugated polymers $PHEMA_{50}$-RA-PCB_{20}-CPP was 41 μg mL^{-1}, which was much lower than that of the $PHEMA_{50}$-PCB_{20}-CPP polymer (85 μg mL^{-1}). These results demonstrate that the conjugation with the hydrophobic RA may enhance the self-assembling ability of polymers. Furthermore, the CMC for the $PHEMA_{50}$-RA-PEG-CPP polymer was 45 μg mL^{-1}, which was comparable to that of $PHEMA_{50}$-RA-PCB_{20}-CPP.

Next, PHEMA-RA-PC*B*-C*P*P/SPIONs/siSOX9 NPs (abbreviated as ABC/SPIONs/siSOX9 NPs) were prepared to study their effect on the differentiation of NSCs. As shown in Table S4 (Supporting Information), PHEMA-RA-PC*B*/SPIONs/siSOX9 NPs without CPP (abbreviation as AB/SPIONs/siSOX9 NPs) were also prepared as comparison to study the effect of CPP on the cellular uptake. Non-pH-sensitive cationic lipid dimethyldioctadecylammonium bromide (DDAB) was used in PHEMA-RA-PE*G*-C*P*P/SPIONs/siSOX9 NPs (abbreviated as AGC/SPIONs/siSOX9 NPs) to adsorb siSOX9. Moreover, RA-encapsulated PHEMA-PC*B*-C*P*P/RA/SPIONs/siSOX9 NPs (abbreviation as BC/A/SPIONs/siSOX9 NPs) were prepared to investigate the effect of the temporally controlled release on the differentiation of NSCs.

To evaluate the siSOX9 complexing ability of the NPs, the buffering capacity of the NPs before complexing with siSOX9 was investigated by acid–base titration in 0.01 M NaCl aqueous solution.[20] As shown in Figure S5A (Supporting Information), PEG-based AGC/SPIONs NPs had no buffering capacity, whereas PCB modification led to a better buffering capacity over the pH range of 7.4 to 3.5. Furthermore, the zeta potential of ABC/SPIONs NPs showed a pH dependency, whereby the zeta potential enhanced from 2.6 mV at pH 7.4 to 15.4 mV at pH 3.5 (Figure S5B, Supporting Information). This means that the protonation of PCB in acidic conditions could enhance the positive charge of the NPs, which in turn enables PCB complexing with siSOX9, like with cationic polymers or lipids.

Next, gel-electrophoresis assay was adopted to evaluate whether PCBylated NPs were capable of absorbing siSOX9 in acidic conditions. As shown in Figure S6 (Supporting Information), PCB-modified NPs could complex with siSOX9 in acidic solutions. As expected, the complexing ability was enhanced under lower pH conditions, whereby ABC/SPIONs NPs achieved complete retardation at a N/P ratio of 3:1 at pH 4, whereas it was at a N/P ratio of 15:1 at pH 6. However, the NPs were unstable at pH values lower than 4 as at this point RA was released due to the breakage of the ester bond. Therefore, we chose pH 4 for the following experiments. Furthermore, as displayed in Figure S7 (Supporting Information), AB/SPIONs NPs, ABC/SPIONs NPs, and BC/A/SPIONs NPs could completely retard siRNA at a N/P ratio of 3:1, 3:1, and 5:1, respectively, at pH 4, which was comparable with that of PEGylated AGC/SPIONs NPs including the cationic lipid DDAB (N/P = 5:1). Moreover, the diameter decreased to about 100 nm at a N/P ratio of 5:1 (**Figure 1**A and Figure S8A, Supporting Information), and the zeta potential reverted to 0.0–3.0 mV after dialysis for PCBylated NPs at a N/P ratio of 5:1 (Figure S8B, Supporting Information). As excess materials may impose an extra burden for patients to excrete, NPs with a N/P ratio of 5:1 were chosen for the following experiments.[21]

The transmission electron microscopy (TEM) images in Figure 1B (i) show that the SPIONs were monodispersed and had a spherical-like structure with a diameter of about 10 nm. They were aggregated at the center of the ABC/SPIONs/siSOX9

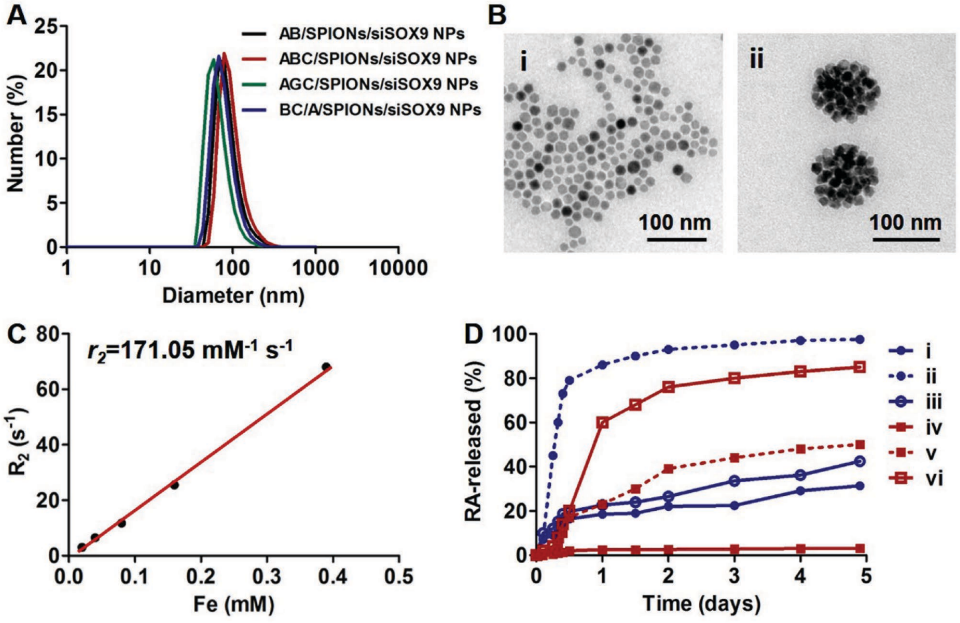

Figure 1. A) The diameter of the NPs at an N/P ratio of 5:1. B) TEM images of SPIONs (i) and ABC/SPIONs/siSOX9 NPs (ii). C) The r_2 value of ABC/SPIONs/siSOX9 NPs. D) The RA released from the NPs at different conditions at 37 °C. For BC/A/SPIONs/siSOX9 NPs: i) pH 7.4, ii) pH 5.0, iii) pH 7.4+esterase; for ABC/SPIONs/siSOX9 NPs: iv) pH 7.4, v) pH 5.0 and vi) pH 7.4+esterase.

NPs after encapsulation (Figure 1B(ii)). To further assess their magnetic property, the r_2 value was calculated by measuring the change in the spin–spin relaxation rate (R_2) per unit iron concentration. As shown in Figure 1C, the ABC/SPIONs/siSOX9 NPs had an r_2 value of 171.05 mM^{-1} s^{-1}, which was high enough for in vivo application.

The loading efficiency of RA was detected using UV–vis spectroscopy with a characteristic absorbance peak at 360 nm. As displayed in Table S5 (Supporting Information), the loading efficiency of RA for the RA-conjugated NPs was comparable, namely it was about 86.67, 86.09, and 84.88 μg mg^{-1} for the AB/SPIONs/siSOX9 NPs, ABC/SPIONs/siSOX9 NPs, and AGC/SPIONs/siSOX9 NPs, respectively. However, the loading efficiency was 68.40 μg mg^{-1} for the BC/A/SPIONs/siSOX9 NPs, which was lower than that of the RA-conjugated NPs, due to their poor assembly ability. To investigate the release kinetics of RA, the NPs were incubated under different conditions for 5 days at 37 °C. The conditions of pH 7.4, 5.0, and 7.4 in the presence of esterase were simulating the culture medium, endosomes/lysosomes, and cytoplasm of the NSCs, respectively. From the release graph in Figure 1D, there was an initial burst release of 18.5% for BC/A/SPIONs/siSOX9 NPs in pH 7.4 after 1 day of incubation (i), indicating that they were unstable in culture medium. The BC/A/SPIONs/siSOX9 NPs were more sensitive to acidic conditions and as a result about 86.0% of the RA was released after 1 day of incubation at pH 5.0 (ii). The reason for this was illustrated in our previous work, in short: the protonation of PCB in acidic conditions results in an extensive disruption of the NPs and thus in the release of the encapsulated drug.[22] The BC/A/SPIONs/siSOX9 NPs were less responsive to the presence of esterase and thus only 22.7% was released after 1 day of incubation (iii). In comparison, the released RA for ABC/SPIONs/siSOX9 NPs was negligible at pH 7.4 (iv), indicating that they were stable in culture medium. Even at pH 5.0 the release was still only 23.1% (v) after 1 day of incubation, whereas it is clear that 60.0% of RA was sustainedly released in PBS-containing esterase (vi). This would be favorable for the temporal controlled release of RA as siSOX9 could then be released earlier in the endosomes/lysosomes in our system and RA would then be released later in the cytoplasm.

To validate this, cultured cells isolated from the hippocampus of suckling-mice were immunolabeled with markers including Nestin, sex-determining region y-box 2 (Sox2), and immature neuronal marker doublecortin (DCX). The results demonstrated that the NSCs were positively marked (Figure S9, Supporting Information). Before in vivo application, the biocompatibility of the NPs on NSCs was studied using a methyl thiazolyl tetrazolium (MTT) asay. As illustrated in Figure S10 (Supporting Information), the cell viability was above 92% at an N/P ratio of 5:1 for all NPs. The apoptosis of NSCs after treatment with NPs (N/P = 5:1) was further evaluated by Annexin V/PI assay. As shown in Figure S11 (Supporting Information), compared to the PBS control groups, there was no significant cell apoptosis of NSCs after treatment with NPs (N/P = 5:1), which rendered them suitable for applications.

Furthermore, the internalization of NPs was analyzed by flow cytometry using carboxyfluorescein (FAM)-labeled siRNA (FAM-siRNA) as a fluorescence probe (**Figure 2**A). CPP is shown to enhance the interaction between the NPs and the NSCs as the mean fluorescence intensity (MFI) of the ABC/SPIONs/FAM-siRNA NPs was 1.6 times that of the AB/SPIONs/FAM-siRNA NPs. The MFI of ABC/SPIONs/FAM-siRNA NPs was also much stronger than that of BC/A/SPIONs/FAM-siRNA NPs because of their higher stability in culture medium. Surprisingly, the cellular uptake of ABC/SPIONs/FAM-siRNA NPs was much higher than that of AGC/SPIONs/FAM-siRNA NPs. To illustrate this, the interactions between NSCs and NPs were observed by spinning disk confocal imaging. The results (Figure 2B and Video 1–2, Supporting Information) showed that extensive filopodia protruded from the NSCs after incubation with ABC/SPIONs/FAM-siRNA NPs, whereas there was almost no filopodia observed from the NSCs after incubation with AGC/SPIONs/FAM-siRNA NPs. To further understand the mechanism, we characterized the actin cytoskeleton after treatment with NPs. Cells treated with PEGylated NPs exhibited nearly spherical actin skeletons (Figure 2C(i)), whereas NSCs treated with ABC/SPIONs/siSOX9 NPs displayed extended actin skeletons (white arrow, Figure 2C(ii)). The filopodia enhanced the cellular uptake because of their active capturing ability. This difference might be attributed to the different topographical structure in which the nano-brushed PCB may enhance the topographic interactions between the NPs and the nanoscaled filopodia of the NSCs.[23] Furthermore, the distribution of SPIONs in the NSCs was observed by TEM (Figure 2D). Figure 2D(i) demonstrates the presence of electron-dense SPIONs (red circle) in the NSCs after treatment with ABC/SPIONs/siSOX9 NPs for 4 h and the electron-dense spots of SPIONs were also visible under high-magnification visualization. Although the control NSCs also showed electron-dense black spots (Figure 2D(ii), red circle), the spots in the untreated NSCs were proven to be non-specific under high-magnification visualization.[24]

After endocytosis in the NSCs, siSOX9 was expected to be released earlier than RA to down-regulate the expression of the SOX9 protein in advance. The endosomal/lysosomal escape of the NPs was observed with CLSM, whereby the blue fluorescence is the autofluorescence of RA at an excitation wavelength of 405 nm. As shown in Figure 2E, there were a relatively high number of co-localization (white) spots for AB/SPIONs/FAM-siRNA NPs and ABC/SPIONs/FAM-siRNA NPs after 4 h of incubation, which combined the green FAM-siRNA, blue RA, and red endosomes/lysosomes fluorescence. However, the co-localization spots were yellow for the AGC/SPIONs/FAM-siRNA and BC/A/SPIONs/FAM-siRNA NPs because of their poor cellular uptake. These results indicated that the majority of the RA and FAM-siRNA was located within the endosomes/lysosomes for all NPs. After 8 h of incubation, the FAM-siRNA fluorescence started to be separated from the endosomes/lysosomes for the AB/SPIONs/FAM-siRNA NPs and the ABC/SPIONs/FAM-siRNA NPs because of the proton-buffering effect of PCB in acidic environment, and the co-localization ratio was reduced by 22.0% and 21.7%, respectively (Figure S12, Supporting Information). Additionally, no RA blue fluorescence was observed in the nucleus for both NPs. However, the green FAM-siRNA fluorescence of the AGC/SPIONs/FAM-siRNA NPs was still co-localized with the red fluorescence and the co-localization ratio only reduced by 2.0%, suggesting that

Adv. Mater. **2016**,
DOI: 10.1002/adma.201600554

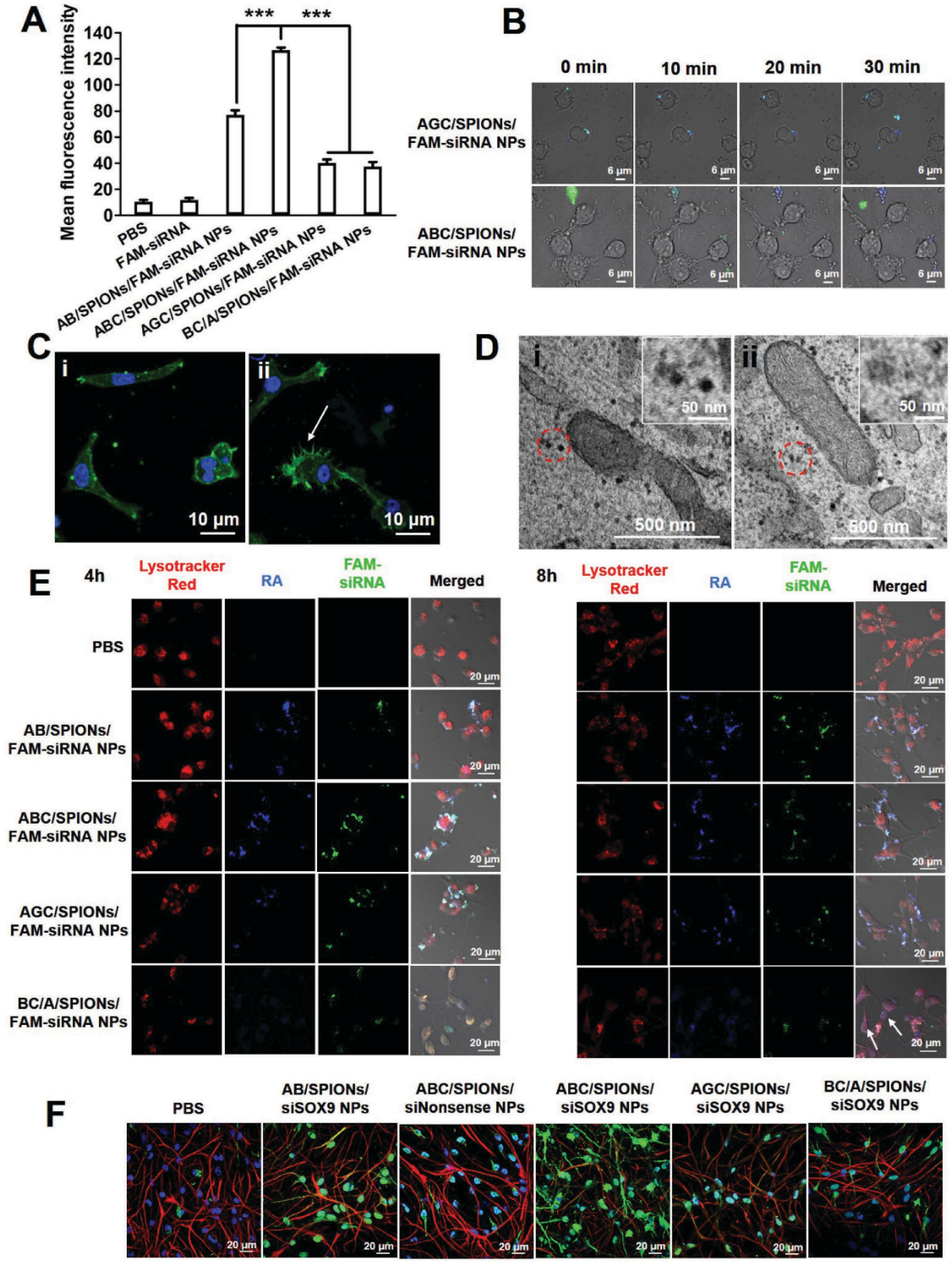

Figure 2. A) Cellular uptake of NPs after incubation in culture medium for 3 h detected by flow cytometry. B) Spinning disk confocal image of NSCs following incubation with NPs. C) Immunofluorescent images including actin (green) and the nucleus (blue) of the NSCs after 0.5 h of incubation with NPs. i) AGC/SPIONs/siSOX9 NPs, ii) ABC/SPIONs/siSOX9 NPs. D) TEM of an ultrathin section of NSCs incubated with ABC/SPIONs/siSOX9 NPs (i) or PBS (ii) for 4 h. The images in the inset are the electron-dense dark spots (red circle) observed under high-magnification visualization. E) Assessment by CLSM of the endosomal/lysosomal escape of NPs in NSCs after 4 h and 8 h of incubation. Endosomes/lysosomes were stained with lysotracker red with an excitation wavelenght of 534 nm. siRNA was labeled with FAM with an excitation wavelength of 488 nm. The blue fluorescence is the autofluorescence of RA with an excitation wavelength of 405 nm. F) Neural differentiation of NSCs treated with NPs for 10 days. The cells were immunostained with MAP-2 (green) for the neurons, GFAP (red) for glial cells, and DAPI (blue) for nucleus. The mean ± SD is shown. ***$P < 0.005$ ($n = 3$) versus control.

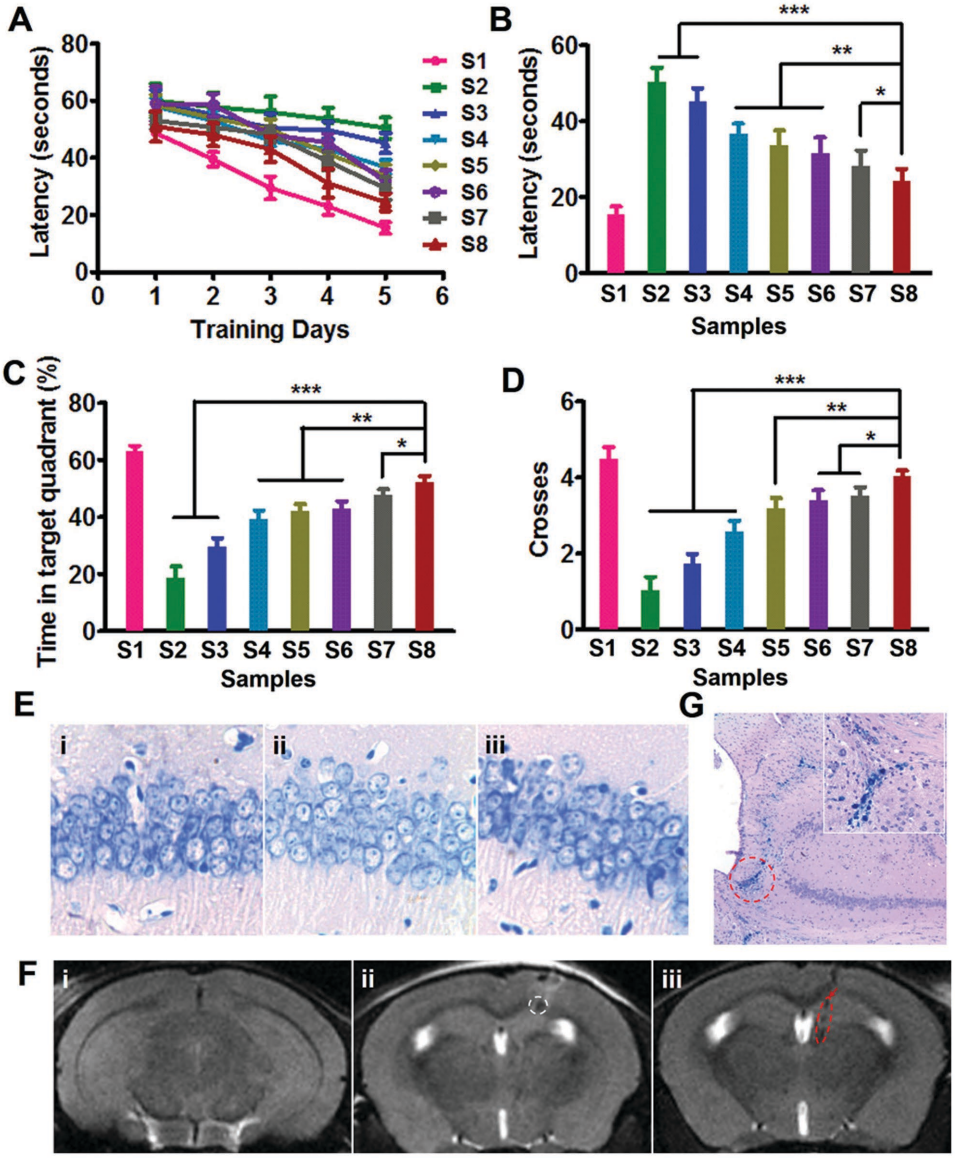

Figure 3. A) The escape latency of 2×Tg-AD mice treated with different formulations. B) The latency during the memory test in a MWM probe trial without a platform. C) The percentage of time in the target quadrant with a platform included in the MWM. D) The number of 2×Tg-AD mice that crossed the platform in the target quadrant where the platform had been located during the MWM. Key: S1) wild, S2) PBS, S3) NSCs alone, S4) ABC/SPIONs/siNonsense NPs NSCs, S5) BC/A/SPIONs/siSOX9 NPs NSCs, S6) AGC/SPIONs/siSOX9 NPs NSCs, S7) AB/SPIONs/siSOX9 NPs NSCs, and S8) ABC/SPIONs/siSOX9 NPs NSCs. E) Nissl staining of nerve cells in the brains of wild and 2×Tg-AD mice treated with different formulations. Key: i) wild, ii) PBS, iii) ABC/SPIONs/siSOX9 NPs NSCs. F) Representative in vivo T2 MRI images of brains in 2×Tg-AD mice, before (i) and after transplantation of NSCs with ABC/SPIONs/siSOX9 NPs for 1 day (ii) and 35 days (iii). G) Prussian-blue staining of nerve cells in brains of 2×Tg-AD mice treated with ABC/SPIONs/siSOX9 NPs. The inset image is the staining (red circle) observed under high-magnification visualization. The mean ± SD is shown. $*P < 0.05$, $**P < 0.01$, and $***P < 0.005$ ($n = 5$) versus control.

FAM-siRNA was still mainly located within the endosomes/lysosomes because of the steric hindrance of PEG. In comparison, although RA-encapsulated BC/A/SPIONs/FAM-siRNA NPs could achieve fast endosomal/lysosomal escape of FAM-siRNA with a co-localization ratio decrease of 23.0%, RA was simultaneously released into the nucleus (white arrow). The release kinetics of FAM-siRNA from all NPs of all internalized FAM-siRNA at various time points also confirmed the expedited endosomal/lysosomal escape of PCB-modified NPs (Figure S13, Supporting Information). The release was approximately 80.0% for PCB-based NPs, whereas only 53.4% was achieved for PEG-based AGC/SPIONs/FAM-siRNA NPs after 8 h of incubation. As expected, only RA-conjugated NPs modified with PCB met the requirement of releasing siRNA earlier into the acting site than RA.

To test whether the ABC/SPIONs/siSOX9 NPs with better cellular uptake and endosomal/lysosomal escape could indeed deregulate the expression of SOX9, the actual down-regulation ability was measured by room-temperature polymerase chain reaction (RT-PCR). As shown in Figure S14 (Supporting

Adv. Mater. **2016**,
DOI: 10.1002/adma.201600554

Information), the ABC/SPIONs/siSOX9 NPs could indeed significantly silence the gene expression of SOX9 in NSCs, leading to a knock-down of approximately 52.3% of SOX9 mRNA, which was better than the negative controls.

To further analyze the effects of our NPs on neuronal differentiation, the cells were characterized via immunolabelling with microtubule-associated protein 2 (MAP-2) to label the neurons (green) and glial fibrillary acidic protein (GFAP) to label the glial cells (red). As displayed in Figure 2F and Figure S15 (Supporting Information), in the PBS control cells the majority of NSCs differentiated into glial cells (89.0% GFAP MFI) rather than into neurons (11.0% MAP-2 MFI). Free siSOX9 had almost no effect on the controlled differentiation of the NSCs to neurons because of its poor cellular uptake. Although RA could promote the differentiation of NSCs to neurons, its effect was limited (Figure S16, Supporting Information). However, treatment with NPs resulted in a higher MAP-2 MFI compared to that in the control. Among these, the NSCs treated with ABC/SPIONs/siSOX9 NPs exhibited the highest MAP-2 MFI at 76.8%, which could be attributed to the better cellular uptake of the NPs and the synergistic effect with the temporally controlled release of siSOX9 and RA.

Morris water maze (MWM) experiments were performed to examine whether the NSCs treated with NPs could improve the spatial learning and memory of APPswe/PS1dE9 double transgenic mice (2×Tg-AD). As expected, the mice treated with ABC/SPIONs/siSOX9 NPs NSCs (S8) had shorter escape latencies after 1 to 5 days (**Figure 3**A) and significantly shorter latencies at 1 month after NSCs transplantation (Figure 3B), indicating that the ABC/SPIONs/siSOX9 NPs NSCs could significantly improve the cognition and memory of 2×Tg-AD mice. These results were further confirmed by the fact that mice treated with ABC/SPIONs/siSOX9 NPs NSCs spent more time in the target quadrant (Figure 3C) and crossed the former platform location significantly more than the other groups (Figure 3D). Neuronal loss in the hippocampus is one of the key hallmarks of AD. The Nissl staining analysis in Figure 3E shows that compared to wild mice (i), neuronal hypocellularity and neuron nuclear shrinkage were observed in the hippocampus of 2×Tg-AD mice treated with PBS (ii). After treatment with ABC/SPIONs/siSOX9 NPs NSCs (iii), there were more neurons again, indicating that the neurons recovered their integrity in AD mice.

During the therapeutic process, the traceability in vivo was observed using T2 MRI after treating the NSCs with ABC/SPIONs/siSOX9 NPs. As shown in Figure 3F, 1 day after transplantation the difference in position of the NSCs with ABC/SPIONs/siSOX9 NPs in the ventricular system compared to that before transplantation (Figure 3F(i)) could be seen by MRI (Figure 3F(ii), white circle). The subsequent MRI, taken after 5 weeks, shows that the NSCs extended posteriorly from the injection site into the hippocampus (Figure 3F(iii), red arrow and circle). These results were further confirmed by Prussian-blue staining, showing that SPIONs were distributed in the hippocampus (Figure 3G). In general, our results have demonstrated that NSCs treated with ABC/SPIONs/siSOX9 NPs could achieve long-term monitoring of NSCs and significantly improve the learning and memory of AD mice.

In summary, we constructed charge-reversible PCB-based therapeutic and traceable ABC/SPIONs/siSOX9 NPs that integrate the functionalities of cationic materials and PEG. On the one hand, the modification of CPP enhanced the interaction between the NSCs and the NPs. And on the other hand, extensive filopodia protruded from the NSCs after incubation with ABC/SPIONs/siSOX9 NPs because of the enhanced topographic interaction between the nano-brushed PCB and the NSCs. These two factors resulted in a better cellular uptake. In addition, we have shown that siSOX9 can be controllably released from the NPs in the endosomes/lysosomes because of the protonation of PCB before RA is released in the cytoplasm. Because of their superior cellular uptake and temporally controlled release ability, ABC/SPIONs/siSOX9 NPs could efficiently control the differentiation of NSCs to neurons, which resulted in ameliorating neurologic changes and better rescuing the memory deficits in 2×Tg-AD mice. Moreover, the system allowed the monitoring of the transplantation site and the migration of the NSCs after transplantation because of the high r_2 value of the SPIONs. Therefore, these traceable ABC/SPIONs/siSOX9 NPs might have the potential to open up a new avenue for treatment applications for AD as well as other neurodegenerative disorders because of their excellent tracing and therapeutic ability.

Supporting Information

Supporting Information is available from the Wiley Online Library or from the author.

Acknowledgements

R.Z. and Y.L. contributed equally to this work. This work was financially supported by the National Natural Science Foundation of China (31522023, 51373177, 31470961), the National High Technology Research and Development Program (2014AA020708), the Instrument Developing Project of the Chinese Academy of Sciences (YZ201313), the "Strategic Priority Research Program" of the Chinese Academy of Sciences (XDA09030301-3), the Beijing National Science Foundation (Z141100000214010), the Key Basic Research Special Foundation of Science Technology Ministry of Hebei Province (14961302D), the Hebei Province "Hundred Talents Program" (BR2-202) and the Hebei Province "Three Three Three Talents Program" (A201401002). All procedures involving experimental animals were performed in accordance with protocols approved by the Institutional Animals Care and Use Committee of Peking University.

Received: January 29, 2016
Revised: April 12, 2016
Published online:

[1] a) R. R. Ager, J. L. Davis, A. Agazaryan, F. Benavente, W. W. Poon, F. M. LaFerla, M. Blurton-Jones, *Hippocampus* **2015**, *25*, 813; b) M. Li, X. J. Yang, J. S. Ren, K. G. Qu, X. G. Qu, *Adv. Mater.* **2014**, *24*, 1722.

[2] a) W. Li, T. Guan, X. Zhang, Z. Wang, M. Wang, W. Zhong, H. Feng, M. Xing, J. Kong, *ACS Appl. Mater. Interfaces* **2015**, *7*, 3018; b) M. Blurton-Jones, B. Spencer, S. Michael, N. A. Castello, A. A. Agazaryan, J. L. Davis, F. J. Müller, J. F. Loring, E. Masliah, F. M. LaFerla, *Stem Cell Res. Ther.* **2014**, *5*, 46.

[3] a) T. H. Kim, C. H. Yea, S. D. Chueng, P. T. Yin, B. Conley, K. Dardir, Y. Pak, G. Y. Jung, J. W. Choi, K. B. Lee, *Adv. Mater.* **2015**, *27*, 6356;

b) T. T. Yin, L. C. Yang, Y. N. Liu, X. B. Zhou, J. Sun, J. Liu, *Acta Biomater.* **2015**, *25*, 172.
[4] a) P. Guha, J. W. Morgan, G. Mostoslavsky, N. P. Rodrigues, A. S. Boyd, *Cell Stem Cell* **2013**, *12*, 407; b) Z. Wang, Y. Wang, Z. Y. Wang, J. Zhao, J. S. Gutkind, A. Srivatsan, G. F. Zhang, H. S. Liao, X. Fu, A. Jin, X. Tong, G. Niu, X. Y. Chen, *ACS Nano* **2015**, *9*, 6683; c) C. N. Zhao, G. Q. Sun, S. X. Li, M. F. Lang, S. Yang, W. D. Li, Y. H. Shi, *Proc. Natl. Acad. Sci. USA* **2010**, *107*, 1876.
[5] V. Darsalia, S. J. Allison, C. Cusulin, E. Monni, D. Kuzdas, T. Kallur, O. Lindvall, Z. Kokaia, *J. Cerebr. Blood F. Met.* **2011**, *31*, 235.
[6] S. Y. Park, J. Park, S. H. Sim, M. G. Sung, K. S. Kim, B. H. Hong, S. Hong, *Adv. Mater.* **2011**, *23*, H263.
[7] M. Blurton-Jones, M. Kitazawa, H. Martinez-Coria, N. A. Castello, F. J. Muller, J. F. Loring, T. R. Yamasaki, W. W. Poon, K. N. Green, F. M. LaFerla, *Proc. Natl. Acad. Sci. USA* **2009**, *106*, 13594.
[8] X. Wen, Y. Wang, F. Zhang, X. Zhang, L. Lu, X. T. Shuai, J. Shen, *Biomaterials* **2014**, *35*, 4627.
[9] a) T. Chu, H. Zhou, T. Wang, L. Lu, F. Li, B. Liu, X. Kong, S. Feng, *Brain Res.* **2015**, *1596*, 31; b) R. C. Schugar, P. D. Robbins, B. M. Deasy, *Gene Ther.* **2008**, *15*, 126.
[10] T. Berbasova, M. Nosrati, C. Vasileiou, W. Wang, K. S. Lee, I. Yapici, J. H. Geiger, B. Borhan, *J. Am. Chem. Soc.* **2013**, *135*, 16111.
[11] a) S. Shah, A. Solanki, P. K. Sasmal, K. B. Lee, *J. Am. Chem. Soc.* **2013**, *135*, 15682; b) C. C. Stolt, P. Lommes, E. Sock, M. C. Chaboissier, A. Schedl, M. Wegner, *Gene Dev.* **2003**, *17*, 1677.
[12] Y. L. Zhang, J. M. Pelet, D. A. Heller, Y. Z. Dong, D. L. Chen, Z. Gu, B. J. Joseph, J. Wallas, D. G. Anderson, *Adv. Mater.* **2013**, *25*, 4641.
[13] a) Y. Li, R. Liu, J. Yang, G. Ma, Z. Zhang, X. Zhang, *Biomaterials* **2014**, *35*, 9731; b) J. G. Li, X. S. Yu, Y. Wang, Y. Y. Yuan, H. Xiao, D. Cheng, X. T. Shuai, *Adv. Mater.* **2014**, *26*, 8217; c) M. Z. Zhang, A. Ishii, N. Nishiyama, S. Matsumoto, T. Ishii, Y. Yamasaki, K. Kataoka, *Adv. Mater.* **2009**, *21*, 3520.
[14] a) B. Hu, F. Dai, Z. Fan, G. Ma, Q. Tang, X. Zhang, *Adv. Mater.* **2015**, *27*, 5499; c) M. Modo, D. Cash, K. Mellodew, S. C. R. Williams, S. E. Fraser, T. J. Meade, J. Price, H. Hodges, *NeuroImage* **2002**, *17*, 803; d) P. J. Chen, Y. D. Kang, C. H. Lin, S. Y. Chen, C. H. Hsieh, Y. Y. Chen, C. W. Chiang, W. Lee, C. Y. Hsu, L. D. Liao, C. T. Fan, M. L. Li, W. C. Shyu, *Adv. Mater.* **2015**, *27*, 6488.
[15] R. Guzman, N. Uchida, T. M. Bliss, D. He, K. K. Christopherson, D. Stellwagen, A. Capela, J. Greve, R. C. Malenka, M. E. Moseley, T. D. Palmer, G. K. Steinberg, *Proc. Natl. Acad. Sci. USA* **2007**, *104*, 10211.
[16] a) T. Santos, R. Ferreira, J. Maia, F. Agasse, S. Xapelli, L. Cortes, J. Bragança, J. O. Malva, L. Ferreira, L. Bernardino, *ACS Nano* **2012**, *6*, 10463; b) S. H. Bakhru, E. Altiok, C. Highley, D. Delubac, J. Suhan, T. K. Hitchens, C. Ho, S. Zappe, *Int. J. Nanomed.* **2012**, *7*, 4613.
[17] a) Z. Rehman, I. S. Zuhorn, D. Hoekstra, *J. Controlled Release* **2013**, *166*, 46; b) R. Wang, R. Xiao, Z. W. Zeng, L. Xu, J. J. Wang, *Nanomedicine* **2012**, *7*, 4185; c) T. M. Sun, J. Z. Du, L. F. Yan, H. Q. Mao, J. Wang, *Biomaterials* **2008**, *29*, 4348.
[18] a) C. L. Chan, R. N. Majzoub, R. S. Shirazi, K. K. Ewert, Y. J. Chen, K. S. Liang, C. R. Safinya, *Biomaterials* **2012**, *33*, 4928; b) H. Hatakeyama, H. Akita, K. Kogure, M. Oishi, Y. Nagasaki, Y. Kihira, M. Ueno, H. Kobayashi, H. Kikuchi, H. Harashima, *Gene Ther.* **2007**, *14*, 68.
[19] Y. Li, Q. Cheng, Q. Jiang, Y. Y. Huang, H. M. Liu, Y. L. Zhao, W. P. Cao, G. H. Ma, F. Y. Dai, X. J. Liang, Z. C. Liang, X. Zhang, *J. Controlled Release* **2014**, *176*, 104.
[20] E. Tombácz, Z. Libor, E. Illés, A. Majzik, E. Klumpp, *Org. Geochem.* **2004**, *35*, 257.
[21] a) Y. Wen, S. Jin, *J. Biotechnol.* **2014**, *188*, 122; b) Y. Shen, E. Jin, B. Zhang, C. J. Murphy, M. Sui, J. Zhao, J. Wang, J. Tang, M. Fan, E. Van Kirk, W. J. Murdoch, *J. Am. Chem. Soc.* **2010**, *132*, 4259.
[22] Y. Li, R. Y. Liu, J. Yang, Y. J. Shi, G. H. Ma, Z. Z. Zhang, X. Zhang, *Biomaterials* **2015**, *41*, 1.
[23] L. E. Hebert, J. Weuve, P. A. Scherr, D. A. Evans, *Neurology* **2013**, *80*, 1778.
[24] R. Pahuja, K. Seth, A. Shukla, R. K. Shukla, P. Bhatnagar, L. K. S. Chauhan, P. N. Saxena, J. Arun, B. P. Chaudhari, D. K. Patel, S. P. Singh, R. Shukla, V. K. Khanna, P. Kumar, R. K. Chaturvedi, K. C. Gupta, *ACS Nano* **2015**, *9*, 4850.

Adv. Mater. **2016**,
DOI: 10.1002/adma.201600554